

High-Sensitivity Raman Spectrometer To Study Pristine and Irradiated Interstellar Ice Analogs

Chris J. Bennett,^{‡,§,⊥,†} Stephen J. Brotton,^{‡,§} Brant M. Jones,^{‡,⊥} Anupam K. Misra,[¶] Shiv K. Sharma,[¶] and Ralf I. Kaiser^{*,‡,⊥}

[‡]Department of Chemistry, University of Hawai'i at Mānoa, Honolulu, Hawai'i 96822, United States

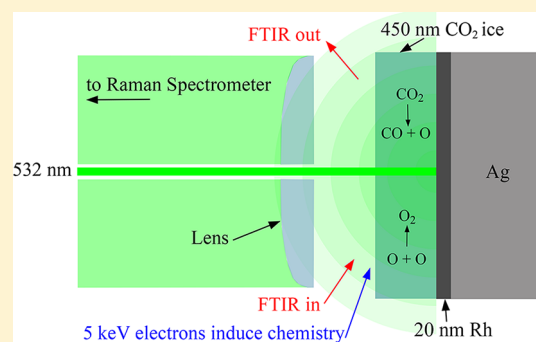
[§]NASA Astrobiology Institute, University of Hawai'i at Mānoa, 2680 Woodlawn Drive, Honolulu, Hawai'i 96822, United States

[⊥]W.M. Keck Research Laboratory in Astrochemistry, University of Hawai'i at Mānoa, Honolulu, Hawai'i 96822, United States

[¶]Hawai'i Institute of Geophysics and Planetology, University of Hawai'i at Mānoa, 2525 Correa Road, Honolulu, Hawai'i 96822, United States

S Supporting Information

ABSTRACT: We discuss the novel design of a sensitive, normal-Raman spectrometer interfaced to an ultra-high vacuum chamber (5×10^{-11} Torr) utilized to investigate the interaction of ionizing radiation with low temperature ices relevant to the solar system and interstellar medium. The design is based on a pulsed Nd:YAG laser which takes advantage of gating techniques to isolate the scattered Raman signal from the competing fluorescence signal. The setup incorporates innovations to achieve maximum sensitivity without detectable heating of the sample. Thin films of carbon dioxide (CO₂) ices of 10 to 396 nm thickness were prepared and characterized using both Fourier transform infrared (FT-IR) spectroscopy and HeNe interference techniques. The ν_+ and ν_- Fermi resonance bands of CO₂ ices were observed by Raman spectroscopy at 1385 and 1278 cm⁻¹, respectively, and the band areas showed a linear dependence on ice thickness. Preliminary irradiation experiments are conducted on a 450 nm thick sample of CO₂ ice using energetic electrons. Both carbon monoxide (CO) and the infrared inactive molecular oxygen (O₂) products are readily detected from their characteristic Raman bands at 2145 and 1545 cm⁻¹, respectively. Detection limits of 4 ± 3 and 6 ± 4 monolayers of CO and O₂ were derived, demonstrating the unique power to detect newly formed molecules in irradiated ices in situ. The setup is universally applicable to the detection of low-abundance species, since no Raman signal enhancement is required, demonstrating Raman spectroscopy as a reliable alternative, or complement, to FT-IR spectroscopy in space science applications.



Icy bodies within the solar system (SS) and the interstellar medium (ISM) are habitually subjected to harsh radiation environments, cold temperatures (as low as 10 K), and often vacuum conditions.^{1–8} Such environments are typically studied within ultra-high vacuum (UHV) chambers at pressures $<1 \times 10^{-9}$ Torr. Ices of volatile species are typically grown in situ via controlled condensation of their gaseous counterparts to thicknesses from monolayers up to several micrometers, though a few hundreds of nm is typical. Here, they are exposed to ionizing radiation which produces small quantities of new chemical species within the bulk of the ices; concentrations of such species vary temporally and spatially throughout the ice depending on the precise nature of the irradiation and target medium and dose they are exposed to. In order to understand the underlying chemical processes, it is necessary to characterize in situ each of the reactive intermediates in addition to the final products formed by the irradiation in not only a qualitative but also a quantitative manner.

Both Fourier transform infrared (FT-IR) and Raman spectroscopy are powerful tools for studying the chemical alteration of low temperature ices during exposure to ionizing radiation.^{1–8} While they both are able to give chemical information regarding the normal vibrational modes, the activity of these modes is based on different, yet complementary, selection criteria. A mode is infrared active if the dipole moment of the molecule changes during the transition. Whereas, a mode is Raman active if the polarizability of the molecule is altered during the transition. Thus, Raman spectroscopy has the unique advantage of being able to detect homonuclear diatomic species such as key interstellar molecules including molecular hydrogen (H₂), molecular oxygen (O₂), molecular nitrogen (N₂), and dicarbon (C₂).⁹ If a molecule possesses an inversion center (center of symmetry), then the

Received: November 8, 2012

Accepted: May 10, 2013

Published: May 10, 2013

Table 1. List of Current Raman Capabilities of Other Laboratories Currently Studying Ice Irradiation Chemistry

Group	Detection System	Excitation Wavelength, nm	Frequency, Hz	Average Power, mW	Sampled Area, μm^2	Average Irradiance, kW cm^{-2}	Reference
The Interstellar Astrochemistry Chamber (Madrid, Spain)	Labram HR800 (Horiba Jobin–Yvon) Raman microscope (ex situ)	514.5	cw	50 ^a	~3	31.83 ^a	36
	iHR550 (Horiba Jobin Yvon)	532.0	cw	N/A	N/A	N/A	37
	RamanRxn1 Analyzer (Kaiser Optical Systems)	532.0	cw	100	N/A	N/A	– ^c
Osservatorio Astrofisico di Catania (Catania, Italy)	SPEX 1488 double monochromator + OMA III (Princeton)	514.5	cw	50	1.26×10^3	0.4–1.2	28
	Triplemate (SPEX)	514.5	cw	50	1.26×10^3	0.4–1.2	69
	Triplemate (SPEX) (ex situ)	514.5	cw	50	~3	31.83 ^b	33
W.M. Keck Laboratory (Honolulu, HI, USA)	PI-MAX2 (Princeton) lens with hole	532.0	1000	201	7.85×10^5	0.03	present study
	PI-MAX2 (Princeton) lens without hole	532.0	1000	201	1.59×10^3	12.64	present study

^aEstimated 1 mW on the sample. ^bEstimated below 0.1 mW on sample. ^cPrivate communication (in development, fiber optics will deliver light to and from the sample).

rule of “mutual exclusion” dictates that no normal mode can be both Raman and infrared active. Consequently in centrosymmetric point groups (such as $D_{\infty h}$, which includes carbon dioxide, CO_2 , and acetylene, C_2H_2), infrared active modes belong to *ungerade* (u) symmetry, whereas Raman active modes must be of *gerade* (g) symmetry.¹⁰ In addition, owing to the different selection rules, vibrational modes which are weak infrared absorbers can on the other hand be strong Raman scatterers (e.g., oxygen–oxygen stretches, $\nu(\text{O}–\text{O})$, double or triple bond carbon–carbon stretches, $\nu(\text{C}\equiv\text{C})$, aromatic ring chain vibrations $\nu(\text{CC})$). Alternatively, weak Raman scatterers can be strong infrared absorbers (e.g., oxygen–hydrogen stretches, $\nu(\text{O}–\text{H})$, asymmetric epoxide stretches, $\nu(\text{C}–\text{O}–\text{C})$).¹¹

The Raman differential scattering cross sections are small for most molecules, typically being of the order of $10^{-30} \text{ cm}^{-2} \text{ sr}^{-1}$ (for comparison, the cross section for a typical infrared absorption is 10^{-19} cm^{-2}).¹² A number of techniques have been developed that effectively increase the Raman scattering cross sections. Considerable progress has been made on surface enhanced Raman scattering (SERS) spectroscopy which, as its name implies, relies on interactions between surfaces roughened on the atomic scale and is highly pronounced when the surface used is gold (Au), silver (Ag), or copper (Cu).^{13–17} In general, two separate mechanisms are believed to enhance the signal, namely, electromagnetic (EM) and chemical (CE). The EM mechanism is often referred to as an antenna-like effect, since the incoming laser light excites localized surface plasmon resonances which generate an amplifying effect directed toward certain “hot spots”: nano-scale-sized peaks, gaps, or crevices which may be prevalent on roughened surfaces, colloidal particles, or specialized substrates.^{18,19} In such regions, enhancement of single molecule cross sections by a factor of up to 10^{10} – 10^{11} have been reported,¹³ thus accounting for the large intensity of the observed signal despite only a small percentage (<0.001%) of molecules contributing;^{15,21} though the average observed enhancement is typically on the order of 10^4 – 10^6 .^{13,19} Tip enhanced Raman spectroscopy (TERS) quintessentially reverses this processes by using a modified scanning electron microscope, which features a nanoscale tip that can be used to focus the laser light to give an enhanced signal that can be rastered over a surface.²⁰ The CE mechanism, in contrast, refers to specific chemical changes that occur when an adsorbate

interacts with the substrate, which can increase the polarization of the molecule or facilitate excitation through charge-transfer processes.²¹ The enhancement factor observed for CE is analyte and substrate dependent, but varies from perhaps a factor of 2 to 10^4 , and operates even when smooth surfaces are used.^{22,23} If the excitation laser wavelength coincides with specific electronic transitions within the analyte, then resonance Raman scattering (RRS) can additionally increase the Raman cross section by a factor of up to 10^6 (particularly for dyes such as Rhodamine 6G, azodyes, and their derivatives),^{13,24,25} which is often a necessity for single molecule detection. Note that SERS, TERS, and RRS typically require specific conditions for the enhancement to be efficient. RRS may not be effective for a wide range of analytes; SERS inherently cannot detect species within the bulk of an ice, since the enhancement only occurs on the substrate, and TERS is effective only on the ice surface (TERS) interface. In addition, the degree of enhancement is often unpredictable, and so these techniques are not routinely utilized for quantitative measurements.¹³ The focus henceforth will be on unenhanced normal Raman spectroscopy.

The Raman effect is inherently a scattering based phenomenon and, as such, requires light collecting optics close to the sample. However, the outgassing properties of most materials prohibits the use of complex optics in UHV conditions.²⁶ The incorporation of UHV-compatible fiber optics may be used for light collection, but these suffer the disadvantage that the long length of fused silica material guiding the light produces a strong Raman signal itself thus complicating sensitive detection.²⁷ Thus, there are very few experimental setups that have successfully managed to incorporate Raman spectroscopy to study radiation chemistry of astrophysical ices, in real time and in situ, whereas FT-IR spectroscopy is commonplace.^{1–8} Research groups studying radiation chemistry that have incorporated Raman spectroscopy to-date are given in Table 1. The first in situ experimental apparatus designed for this purpose was introduced by Spinella et al. (1991).²⁸ However, the sensitivity of this setup is quite limited, since the Raman spectra only demonstrated the ability to detect the initial reactants or solid residues left after irradiation and sublimation of the samples;^{29,30} therefore, these studies were not able to distinctly characterize spectral features originating from specific molecular species acting as reactive intermediates or products. Second, commercially available micro-Raman instruments have been exploited for in situ

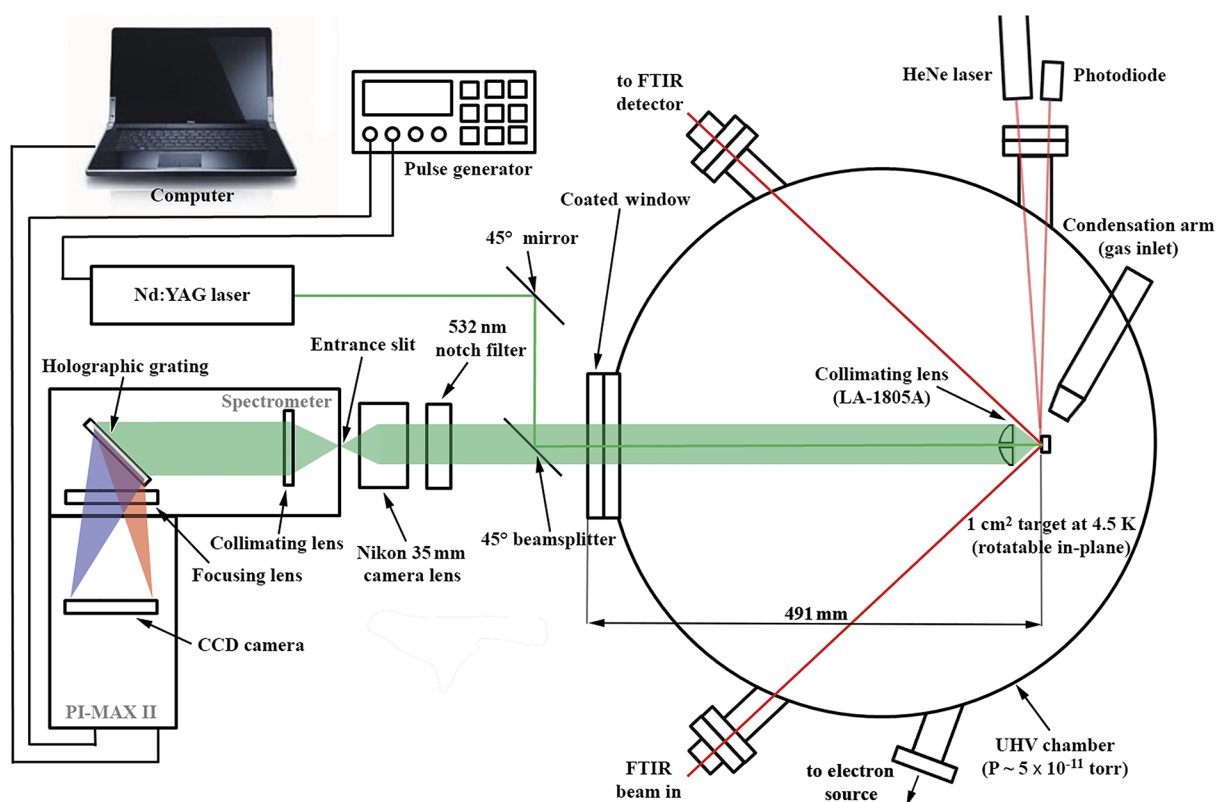


Figure 1. Schematic view of the experimental apparatus.

studies of thin films of amorphous and crystalline water-ice on metal surfaces.^{31,32} However, the use of ex situ micro-Raman instruments to study ion-irradiated ices outside of the vacuum chamber is more commonplace (e.g., Ref 33); but this approach eradicates the possibility of studying unstable species and chemical alteration processes. Furthermore, contamination of the samples occurs when warmed up to room temperature and exposed to the atmosphere. Micro-Raman instruments have also been employed in the characterization of micrometeorites^{34,35} and cometary dust samples.^{36,37}

Here, we present a novel design of a sensitive Raman spectrometer interfaced to an UHV chamber capable of studying the interaction of ionizing radiation with thin ices at temperatures as low as 4.5 K and detecting newly formed molecules via Raman spectroscopy quantitatively in real time and in situ. This setup is able to detect low concentrations of molecules without any enhancements of the Raman signal by SERS, TERS, or RRS. The present apparatus therefore has the advantage of generality, that is, the capability of studying all molecules at different locations of the ice, not only on the ice surface or the ice/substrate interface. We also present preliminary data demonstrating the instrument's ability to detect infrared-inactive irradiation products such as homopolar molecular oxygen (O_2) in experiments, where thin films of CO_2 have been condensed and subsequently irradiated with energetic electrons. While a number of UHV Raman setups exist that are capable of detecting monolayer quantities of analytes,^{16,38–40} to our knowledge, none incorporate radiation sources enabling the study of molecules produced in situ.

EXPERIMENTAL SECTION

Raman Spectrometer Design. The overall design of the Raman spectrometer is depicted in Figure 1. The laser system

utilizes the second harmonics output of a diode-pumped, Q-switched Nd:YAG laser emitting at 532 nm (Crystalaser; QL532-1W) which is triggered at 1 kHz by a pulse generator (Quantum Composers; 9518+). The beam with a diameter of 0.35 mm and a 3.8 mrad divergence is emitted at a pulse width of 13.5 ns at pulse energies of 200 μ J and is reflected from a 45° mirror (Edmund Optics; NT45-991, >99% reflectance) toward a 45° RazorEdge dichroic beamsplitter (Semrock; LPD01-532RU-25 \times 36 \times 2.0). This beam splitter reflects the laser beam toward the sample; on the return path, it transmits the longer Raman-shifted wavelengths. The laser beam enters the UHV chamber through a 4.5 in. conflat (CF) UHV compatible viewport (Kurt J. Lesker; VPZL-450DUC2; 425–760 nm) equipped with antireflection coating on both sides of the window. The laser pulse travels approximately 0.5 m before reaching the sample ice, which was condensed from the gas phase via controlled chemical vapor deposition (see Supporting Information for additional details). Samples are condensed onto a surface with an area of 1.27 cm \times 1.27 cm that consists of silver polished to a mirror finish coated with a 20 nm thick layer of rhodium. This suppresses SERS enhancement at the ice/substrate interface and extends the reflectivity at lower wavelengths enabling the study of ices with UV-VIS spectroscopy in future applications. The sample is freely rotatable and can be cooled down to 4.5 K by a closed cycle 2-stage helium refrigerator (Sumitomo; RDK-408D2). On its path to the sample, the laser pulse passes through a hole of 1.0 mm diameter drilled through the center of a plano-convex lens (Thorlabs; LA1805-A; diameter ϕ = 25.4 mm; focal length = 30.0 mm with antireflection coating), which is mounted on a translation stage (\pm 5 mm travel). The purpose of the lens is to collimate the scattered signal back toward the viewport. The hole ensures that the laser beam is not focused onto the ice

sample. Note that trial lenses that did not feature the central hole were tested, which focused the laser beam to a smaller spot on the sample ($\varnothing \sim 45 \mu\text{m}$). While similar sensitivity could be obtained, the increased power density was sufficient to promote sublimation of the sample and also laser induced breakdown of the target ice.⁴¹ Studies on the angular dependence of Raman scattering intensity demonstrate that the lens should be placed in a backward-scattered orientation, relative to the incoming laser beam to achieve the maximum signal.^{42,43} The mirror-quality rhodium surface reflects the laser beam back through the sample and additionally reflects forward-scattered Raman signal that would have been lost back toward the lens. The lens-sample distance is optimized to collimate the light scattered from the sample, which returns through the same 4.5 in. CF viewport as the 532 nm laser beam entered. The 532 nm laser light reflected from the sample holder and the Rayleigh backscattered light are separated from the Raman signal by the beamsplitter and a notch filter (Kaiser optical systems; HSPF-532.0AR-2.0), thus ensuring that very little of the 532 nm light enters the camera system. A 50 mm $f/1.8$ D-AF lens (Nikon; Model 2137) focuses the Raman light through a slit of width $100 \mu\text{m}$, which gives a spectral resolution of approximately 9 cm^{-1} . The beam then enters the HoloSpec $f/1.8$ imaging spectrometer (Kaiser Optical Systems; model 2004500-501). Inside, a collimating lens directs the light toward the holographic transmission grating (Kaiser Optical Systems; Holoplex HPG-532), which simultaneously disperses the Raman spectral signal into two spatially separated halves on the Intensified Charge-Coupled Device (ICCD) detector; the upper half of the detector covers the low-frequency Raman shifts ($168\text{--}2388 \text{ cm}^{-1}$) while the lower half contains the high-frequency Raman shifts ($2265\text{--}4387 \text{ cm}^{-1}$). The light diffracted by the grating was focused by a lens on to the Peltier-cooled (255 K) PI-MAX2 ICCD camera (Princeton Instruments; Model 7397-0037) with 1024×256 pixels, where each pixel has the dimensions of $26 \mu\text{m} \times 26 \mu\text{m}$. The maximum gain of 255 is applied to the ICCD to gather the maximum possible signal. The Raman signal was optimized by adjusting the gate width and the delay time with respect to the laser pulse; while the Raman signal itself is almost spontaneous, the delay for the laser pulse to be generated after it is triggered from the pulse generator must be accounted for along with associated random fluctuations arising from the electronics. For our particular setup, the optimum gate delay before opening the ICCD to collect the signal was found to be 497 ns after the trigger is sent to the laser, and the gate was left open (gate-width) for the optimum time of 43 ns. A detailed discussion of timing sequences and optimization procedures can be found elsewhere.^{44,45} An important consequence of this gated sequence is that, since the ICCD camera is open only when the Raman signal is at its most intense, we are able to collect spectra without significant interference from daylight. Control experiments conducted in total darkness varied by less than 0.2% in measured signal intensity compared to daylight.⁴⁶ The spectra presented in the Results section were collected for approximately 4 min and are the sum of 100 separate images recorded onto the ICCD camera, with each image itself being the result of light collected on the ICCD during 1000 gate openings. Two backgrounds are typically collected; the first records electrical noise from the ICCD detector (dependent on the gain used) which is subtracted from subsequent spectra. The second is a spectrum of the rhodium or aluminum coated target, which is also subtracted from subsequent spectra. The

images are processed for baseline subtraction, removing what remains of the fluorescence signal. The total counts recorded in each pixel are summed perpendicularly to the dispersion axis to give a total intensity (counts), and the dispersion axis is calibrated to a wavenumber scale using the peak positions of known standards (e.g., liquid cyclohexane).

Thickness Monitoring. The thickness monitoring procedure utilizing the HeNe diffraction technique during the production of thin films is detailed in the Supporting Information.

Irradiation Experiments. In order to test whether products produced via irradiation could be identified by Raman spectroscopy, a CO_2 frost of 450 nm thickness was deposited at 4.5 K and subjected to 1 h of irradiation from 5 keV electrons supplied by an electron source (Specs; EQ-22) at an incident angle of 70° relative to the sample normal. The electron beam had a constant current of 100 nA and was rastered over a sampling area of 1.6 cm^2 . This is equivalent to an average dose of 6.6 eV/molecule .

RESULTS

Quantifying the Thicknesses of Carbon Dioxide Ices.

The thicknesses of the carbon dioxide films as determined from the HeNe interference technique are illustrated in Figure S1, Supporting Information, where the actual thicknesses were determined to be 64, 170, 302, and 396 nm with errors ± 5 nm. The corresponding FT-IR spectra at these ice thicknesses are shown in Figure 2a. Here, the ν_2 bending mode can be seen at 658 cm^{-1} , and the ν_3 asymmetric stretch is observed at 2338 cm^{-1} along with its ^{13}C counterpart at 2282 cm^{-1} . The combination bands $\nu_1 + \nu_3$ and $2\nu_2 + \nu_3$ appear at 3708 and 3600 cm^{-1} , respectively. These values are in good agreement with those reported previously.⁴⁷ Also shown in Figure 2a are the FT-IR spectra taken of the thin ice after most of the CO_2 was sublimated at 86.2 K and then recooled to 4.5 K. The best estimate of the film thickness determined from the ν_3 band is $9.7 \pm 2.7 \text{ nm}$, based on the linear regression carried out and uncertainties in the band area.

The Raman spectra for each of the different ice thicknesses are shown in Figure 2b; the only CO_2 bands observed here are due to the interaction between the Raman active ν_1 symmetric stretching mode and the overtone of the $2\nu_2$ symmetric bending mode, which gives rise to a Fermi resonance doublet featuring high-frequency and low-frequency shift components, denoted as ν_+ and ν_- , respectively.⁴⁸ Here, we find these bands at 1385 and 1278 cm^{-1} in good agreement with previous studies of carbon dioxide ices.^{49,50} Since a linear relationship between the band area and film thickness is expected for optically thin samples,^{51,52} a fitting procedure was applied to determine the gradient from the ice thickness versus peak area data for each band, as shown in Figure S2, Supporting Information. The resulting gradients were used to extrapolate the thickness of the thin CO_2 ice sample left after sublimation from the peak areas of each band, which was determined to be $8.5 \pm 3.8 \text{ nm}$ from the ν_+ band and $16.9 \pm 9.0 \text{ nm}$ from the ν_- band. Both of these values are in good agreement with the infrared data, while the weaker ν_- band is less reliable due to the limited signal-to-noise ratio.

Results of Irradiation Experiments. The FT-IR and Raman spectra of the 450 nm thick ice before and after the irradiation with 5 keV electrons are shown in Figure 3. First, let us discuss the results obtained from the FT-IR spectra, as shown in Figure 3a, where several new peaks become visible.

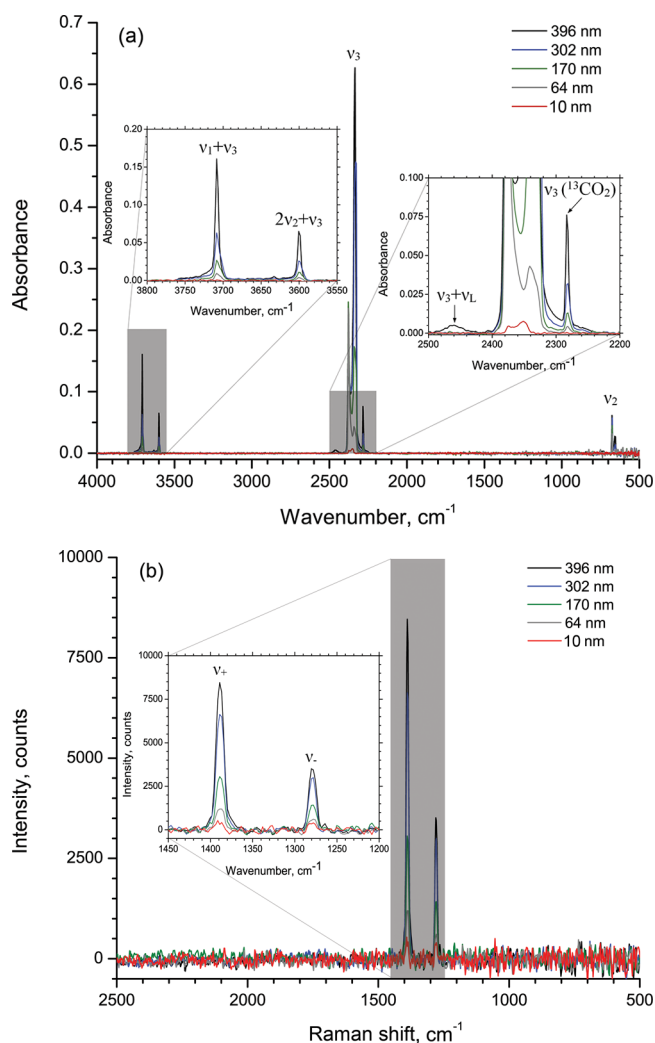


Figure 2. (a) FT-IR spectra over the range of 4000–500 cm⁻¹ and (b) Raman spectra over the range of 2500–500 cm⁻¹ for CO₂ ices of thicknesses of 10 (red), 64 (gray), 170 (green), 302 (blue), and 396 nm (black).

Here, we could identify infrared bands of carbon monoxide (CO; ν_1) at 2139 cm⁻¹ as well as its ¹³C counterpart at 2092 cm⁻¹, carbon trioxide (CO₃; ν_1) at 2044 cm⁻¹, carbon tetraoxide (CO₄; ν_1) at 1940 cm⁻¹, carbon pentaoxide (CO₅; ν_1) at 1912 cm⁻¹, and ozone (O₃; ν_3) at 1042 cm⁻¹, all in good agreement with previous studies.^{47,53,54}

Next, we consider the Raman spectra shown in Figure 3b. Note that the increased number of counts on the ordinate compared to Figure 2b is the result of additional optimization of the apparatus between the two experiments, whereby an increase in the signal-to-noise ratio by a factor of about 6 was made. In Figure 3b, it is possible to identify the formation of two new species, namely, CO at 2145 cm⁻¹ and the infrared inactive O₂ at 1545 cm⁻¹, where both Raman bands correspond to their ν_1 fundamental symmetric stretching vibrations. Again, both of these band positions are in excellent agreement with previous studies where CO(ν_1) has been identified at 2145 cm⁻¹ and O₂(ν_1) at 1553 cm⁻¹.^{55,56} The fact that the fundamental of O₂ is blue-shifted by 8 cm⁻¹ as compared to its position in pure ices is likely interpreted as being due to the formation of a van der Waals complex with another species present within the ice; a similar shift was observed on the

formation of an ON–O₂ complex.⁵⁷ While the identification of CO merely confirms results from the FT-IR measurements, this is the first time that O₂ has been identified by Raman spectroscopy while being formed during irradiation of thin CO₂ ices. The identification of the homonuclear diatomic O₂ as a product formed during the irradiation of CO₂ is made here for the first time by Raman spectroscopy, having not been detectable through FT-IR spectroscopy, although its formation as a precursor to ozone has been implied.^{47,58} Derived lower detection limits for CO and O₂ are given in the Supporting Information.

CONCLUSION

We demonstrated the capabilities of a Raman spectrometer, which has been interfaced to a chamber operating at UHV conditions, in order to study the underlying reaction products formed during the irradiation of thin ice films of astrophysical relevance. Our preliminary studies have shown that this technique is capable of detecting very thin layers (≈ 10 nm) of pristine CO₂ ices, as well as studying in situ the products formed during the irradiation of CO₂ ices, such as CO and O₂, which are typically at concentrations of a few percent of the parent species.⁵⁹ The O₂ represents an example of a homonuclear diatomic molecule not detectable via FT-IR spectroscopy, yet O₂ is an important intermediate required to understand the formation of ozone (O₃) during the irradiation of CO₂ ices.⁴⁷ Here, normal (i.e., nonenhanced) Raman spectroscopy was utilized to detect molecules with typical Raman scattering cross sections present only as minor components of irradiated ices. The identification and quantification of species through Raman spectroscopy can be aided by high-level ab initio and density functional calculations, similar to infrared spectroscopy. Accurate prediction of Raman intensities and band positions in the gas phase can be routinely calculated with modern software.^{60,61} With additional corrections to account for the influence of the surrounding medium, the calculations can be made more representative of the condensed phases.⁶² Anharmonic effects can additionally be accounted for to determine mode-mixing occurrences such as Fermi resonances.⁶³

Since the sensitivity of this instrument has been demonstrated to be comparable to that of traditional FT-IR spectroscopy, it is anticipated that Raman spectroscopy could be more widely utilized within groups studying ice irradiation chemistry, offering an excellent complement or viable alternative to this technique. Further advances could increase the prominence of Raman spectroscopy in routine analysis such as those mentioned in the introduction, as well as coherent anti-Stokes spectroscopy,⁶⁴ or the use of innovative fabricated surfaces such as microcavities.^{65,66} The application of Raman spectroscopy to space-borne missions has only recently commenced. The ChemCam instrument on the Curiosity rover delivered to the martian surface carries a powerful laser-induced breakdown spectrometer (LIBS), which shares similar instrumentation to Raman spectroscopy, for analysis of nearby rocks,⁶⁷ and a similar instrument is proposed for a mission to Saturn's moon, Titan.⁶⁸ Our design for a sensitive Raman spectrometer, which is required to understand the interaction of ionizing radiation with ices, helps open up novel research directions relevant to planetary chemistry.

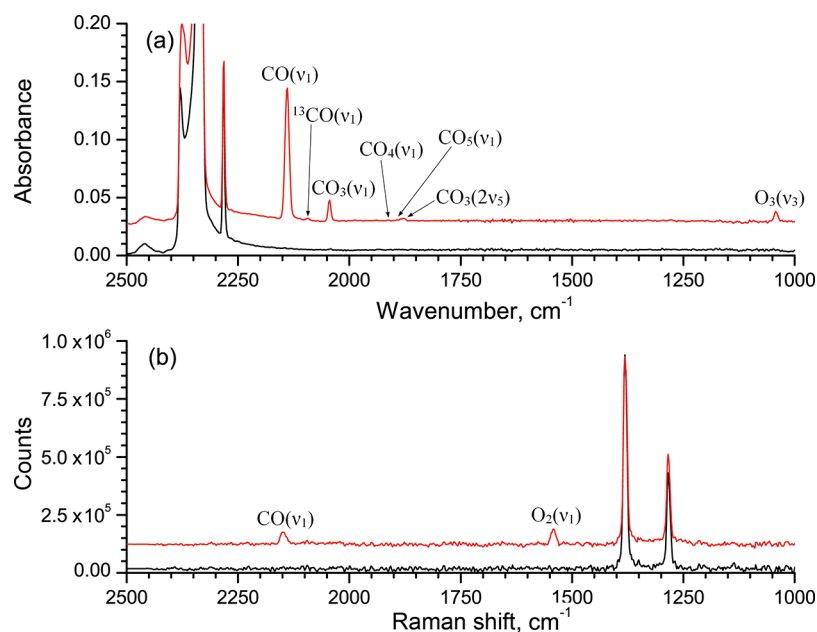


Figure 3. (a) FT-IR and (b) Raman spectra over the wavelength range of 1000–2500 cm^{-1} showing comparisons of an 450 nm thick CO_2 ice before (black) and after (red) irradiation with energetic electrons. New species identified have been labeled.

■ ASSOCIATED CONTENT

Supporting Information

Additional information as noted in text. This material is available free of charge via the Internet at <http://pubs.acs.org>.

■ AUTHOR INFORMATION

Corresponding Author

*E-mail: ralfk@hawaii.edu.

Present Address

†Department of Chemistry and Biochemistry, Georgia Institute of Technology, 901 Atlantic Drive, Atlanta, GA 30332, USA.

Notes

The authors declare no competing financial interest.

■ ACKNOWLEDGMENTS

This project was made possible by the generous financial support of the W. M. Keck Foundation. C.J.B. would like to acknowledge support from the National Aeronautics and Space Administration through the NASA Astrobiology Institute (Cooperative Agreement No. NNA09DA77A issued through the Office of Space Science). We thank the anonymous referee for their valuable suggestions to this work. We also thank Patrick Gasda for his contributions to the initial design and testing of the Raman spectrometer.

■ REFERENCES

- (1) Fraser, H. J.; Collings, M. P.; McCoustra, M. R. S. *Rev. Sci. Instrum.* **2002**, *73* (5), 2161–2170.
- (2) Fuchs, G. W.; Acharyya, K.; Bisschop, S. E.; Öberg, K. I.; van Broekhuizen, F. A.; Fraser, H. J.; Schlemmer, S.; van Dishoeck, E. F.; Linnartz, H. *Faraday Discuss. R. Chem. Soc.* **2006**, *133*, 331–345.
- (3) Fraser, H.; Van Dishoeck, E. *Adv. Space Res.* **2004**, *33* (1), 14–22.
- (4) Hudson, R. L.; Moore, M. H. *Radiat. Phys. Chem.* **1995**, *45* (5), 779–789.
- (5) Allamandola, L.; Sandford, S.; Valero, G. *Icarus* **1988**, *76* (2), 225–252.
- (6) Loeffler, M. J.; Teolis, B. D.; Baragiola, R. A. *J. Chem. Phys.* **2006**, *124*, 104702.

(7) Baratta, G. A.; Leto, G.; Palumbo, M. E. *Astron. Astrophys.* **2002**, *384* (1), 343–349.

(8) Naoki, W.; Akira, K. *Astrophys. J., Lett.* **2002**, *571* (2), L173.

(9) Menten, K.; Wyrowski, F. In *Interstellar Molecules; Springer Tracts in Modern Physics*; Yamada, K. M. T., Winniewisser, G., Eds.; Springer-Verlag: Verline Heidelberg, 2011; Vol. 241, pp 27–42.

(10) Cotton, A. *Chemical Applications of Group Theory*; John Wiley and Sons: New York, 1990.

(11) Socrates, G.; Socrates, G. *Infrared and Raman characteristic group frequencies: tables and charts*; Wiley: Chichester (UK), 2001; Vol. 3.

(12) Aroca, R. *Surface-enhanced vibrational spectroscopy*; Wiley: New York, 2006.

(13) Le Ru, E.; Blackie, E.; Meyer, M.; Etchegoin, P. *J. Phys. Chem. C* **2007**, *111* (37), 13794–13803.

(14) Campion, A.; Kambhampati, P. *Chem. Soc. Rev.* **1998**, *27* (4), 241–250.

(15) Le Ru, E. C.; Etchegoin, P. G. *Annu. Rev. Phys. Chem.* **2012**, *63*, 65–87.

(16) Otto, A.; Mrozek, I.; Grabhorn, H.; Akemann, W. *J. Phys.: Condens. Matter* **1992**, *4* (5), 1143.

(17) Sharma, B.; Frontiera, R. R.; Henry, A.-I.; Ringe, E.; Van Duyne, R. P. *Mater. Today* **2012**, *15* (1), 16–25.

(18) Pemberton, J. E.; Guy, A. L.; Sobocinski, R. L.; Tuschel, D. D.; Cross, N. A. *Appl. Surf. Sci.* **1988**, *32* (1), 33–56.

(19) Fang, Y.; Seong, N.-H.; Dlott, D. D. *Science* **2008**, *321* (5887), 388–392.

(20) Pettinger, B.; Schambach, P.; Villagómez, C. J.; Scott, N. *Annu. Rev. Phys. Chem.* **2012**, *63*, 379–399.

(21) Zhao, L.; Jensen, L.; Schatz, G. C. *J. Am. Chem. Soc.* **2006**, *128* (9), 2911–2919.

(22) Ertürk, Ü.; Otto, A. *Europhys. Lett.* **1988**, *6* (3), 251.

(23) Udagawa, M.; Chou, C.-C.; Hemminger, J.; Ushioda, S. *Phys. Rev. B* **1981**, *23* (12), 6843.

(24) Taylor, G. T.; Sharma, S. K.; Mohanan, K. *Appl. Spectrosc.* **1990**, *44* (4), 635–640.

(25) Xi, K.; Sharma, S. K.; Taylor, G. T.; Muenow, D. W. *Appl. Spectrosc.* **1992**, *46* (5), 819–826.

(26) Moore, J.; Davis, C.; Coplan, M.; Greer, S. *Building Scientific Apparatus*, 3rd ed.; Westview Press: Oxford, U.K., 2002.

(27) Schoen, C.; Cooney, T.; Sharma, S. K.; Carey, D. *Appl. Opt.* **1992**, *31*, 7707–7715.

- (28) Spinella, F.; Baratta, G. A.; Strazzulla, G. *Rev. Sci. Instrum.* **1991**, *62* (7), 1743–1745.
- (29) Court, R. W.; Sephton, M. A.; Parnell, J.; Gilmour, I. *Geochim. Cosmochim. Acta* **2007**, *71* (10), 2547–2568.
- (30) Quirico, E.; Borg, J.; Raynal, P.-I.; Montagnac, G.; d'Hendecourt, L. *Planet. Space Sci.* **2005**, *53* (14–15), 1443–1448.
- (31) Sonwalker, N.; Shyam Sunder, S.; Sharma, S. K. *J. Raman Spectrosc.* **1991**, *22*, 551–557.
- (32) Sonwalker, N.; Sharma, S. K.; Shyam Sunder, S. *Appl. Spectrosc.* **1992**, *46*, 1869–1873.
- (33) Sicilia, D.; Ioppolo, S.; Vindigni, T.; Baratta, G. A.; Palumbo, M. E. *Astron. Astrophys.* **2012**, *543*, A155.
- (34) Busemann, H.; Alexander, M. O. D.; Nittler, L. R. *Meteorit. Planet. Sci.* **2007**, *42* (7–8), 1387–1416.
- (35) Baratta, G. A.; Brunetto, R.; Leto, G.; Palumbo, M. E.; Spinella, F.; Strazzulla, G. *J. Raman Spectrosc.* **2008**, *39* (2), 211–219.
- (36) Muñoz Caro, G. M.; Matrajt, G.; Dartois, E.; Nuevo, M.; d'Hendecourt, L.; Deboffe, D.; Montagnac, G.; Chauvin, N.; Boukari, C.; Du, D. L. *Astron. Astrophys.* **2006**, *459* (1), 147–159.
- (37) Muñoz Caro, G. M.; Dartois, E.; Nakamura-Messenger, K. *Astron. Astrophys.* **2008**, *485* (3), 743–751.
- (38) Champion, A.; Brown, J. K.; Grizzle, V. *Surf. Sci.* **1982**, *115*, 3.
- (39) Matz, D. L.; Pemberton, J. E. *J. Phys. Chem. C* **2012**, *116* (21), 11548–11555.
- (40) Liu, Y.-C.; McCreery, R. L. *J. Am. Chem. Soc.* **1995**, *117* (45), 11254–11259.
- (41) Sharma, S. K.; Misra, A. K.; Lucey, P. G.; Wiens, R. C.; Clegg, S. M. *Spectrochim. Acta, Part A* **2007**, *68* (4), 1036–1045.
- (42) Damen, T. C.; Leite, R. C. C.; Porto, S. P. S. *Phys. Rev. Lett.* **1965**, *14* (1), 9–11.
- (43) Trott, G. R.; Furtak, T. E. *Rev. Sci. Instrum.* **1980**, *51* (11), 1493–1496.
- (44) García, C. S.; Abedin, M. N.; Ismail, S.; Sharma, S. K.; Misra, A. K.; Sandford, S. P.; Elsayed-Ali, H. *Proc. SPIE* **2008**, *6943*, 69430I DOI: 10.1117/12.781458.
- (45) Garcia, C. S.; Abedin, M. N.; Ismail, S.; Sharma, S. K.; Misra, A. K.; Nguyen, T.; Elsayed-Ali, H. *Proc. SPIE* **2009**, *7312*, 731210 DOI: 10.1117/12.818169.
- (46) Misra, A. K.; Sharma, S. K.; Chio, C. H.; Lucey, P. G.; Lienert, B. *Spectrochim. Acta, Part A* **2005**, *61*, 2281–2287.
- (47) Bennett, C. J.; Jamieson, C.; Mebel, A. M.; Kaiser, R. I. *Phys. Chem. Chem. Phys.* **2004**, *6* (4), 735–746.
- (48) Windisch, C. F.; Glezakou, V.-A.; Martin, P. F.; McGrail, B. P.; Schaefer, H. T. *Phys. Chem. Chem. Phys.* **2012**, *14* (8), 2560–2566.
- (49) Cahill, J. E.; Leroi, G. E. *J. Chem. Phys.* **1969**, *51* (4), 1324–1332.
- (50) Sharma, S. K.; Misra, A. K.; Lucey, P. G.; Exarhos, G. J.; Windisch, C. F. *Lunar Planet. Sci. Conf.* **2004**, *35*, 1929.
- (51) Feng, Z. C.; Mascarenhas, A. J.; Choyke, W. J.; Powell, J. A. *J. Appl. Phys.* **1988**, *64* (6), 3176–3186.
- (52) Sovány, T.; Nikowitz, K.; Regdon, G., Jr.; Kása, P., Jr.; Pintye-Hódi, K. *Polym. Test.* **2009**, *28* (7), 770–772.
- (53) Jamieson, C. S.; Mebel, A. M.; Kaiser, R. I. *Chem. Phys. Lett.* **2007**, *440* (1–3), 105–109.
- (54) Jamieson, C. S.; Mebel, A. M.; Kaiser, R. I. *Chem. Phys. Lett.* **2007**, *443* (1–3), 49–54.
- (55) Fenner, W. R.; Hyatt, H. A.; Kellam, J. M.; Porto, S. P. S. *J. Opt. Soc. Am.* **1973**, *63* (1), 73–77.
- (56) Kreutz, J.; Jodl, H. J. *Phys. Rev. B* **2003**, *68* (21), 214303.
- (57) Beckers, H.; Zeng, X.; Willner, H. *Chem.—Eur. J.* **2010**, *16*, 1506–1520.
- (58) Bennett, C. J.; Kaiser, R. I. *Astrophys. J.* **2005**, *635* (2), 1362.
- (59) Bennett, C. J.; Jamieson, C. S.; Osamura, Y.; Kaiser, R. I. *Astrophys. J.* **2006**, *653* (1), 792–811.
- (60) Halls, M. D.; Schlegel, H. B. *J. Chem. Phys.* **1999**, *111* (19), 8819–8824.
- (61) Jimenez-Hoyos, C. A.; Janesko, B. G.; Scuseria, G. E. *Phys. Chem. Chem. Phys.* **2008**, *10* (44), 6621–6629.
- (62) Tomasi, J.; Mennucci, B.; Cammi, R. *Chem. Rev.* **2005**, *105* (8), 2999–3093.
- (63) Seidler, P.; Kongsted, J.; Christiansen, O. *J. Phys. Chem. A* **2007**, *111* (44), 11205–11213.
- (64) Zhang, C.; Wang, J.; Khmaladze, A.; Liu, Y.; Ding, B.; Jasensky, J.; Chen, Z. *Opt. Lett.* **2011**, *36* (12), 2272–2274.
- (65) Sharma, S. K.; Misra, A. K.; Kamemoto, L.; Dykes, A.; Acosta, T. *Proc. SPIE* **2009**, *7313*, 73130F.
- (66) Misra, A. K.; Sharma, S. K.; Kanemoto, L.; Zinin, P. V.; Qigui, Y.; Ningjie, H.; Melnick, L. *Appl. Spectrosc.* **2009**, *63* (3), 373–377.
- (67) Maurice, S.; Wiens, R. C.; Saccoccio, M.; Barraclough, B.; Gasnault, O.; Forni, O.; Mangold, N.; Baratoux, D.; Bender, S.; Berger, G.; Bernardin, J.; Berthé, M.; Bridges, N.; Blaney, D.; Bouyé, M.; Caïs, P.; Clark, B.; Clegg, S.; Cousin, A.; Cremers, D.; Cros, A.; DeFlores, L.; Derycke, C.; Dingler, B.; Dromart, G.; Dubois, B.; Dupieux, M.; Durand, E.; d'Uston, L.; Fabre, C.; Faure, B.; Gaboriaud, A.; Gharsa, T.; Herkenhoff, K.; Kan, E.; Kirkland, L.; Kouach, D.; Lacour, J. L.; Langevin, Y.; Lasue, J.; Mouélic, S.; Lescure, M.; Lewin, E.; Limonadi, D.; Manhès, G.; Mauchien, P.; McKay, C.; Meslin, P. Y.; Michel, Y.; Miller, E.; Newsom, H. E.; Orttner, G.; Paillet, A.; Parès, L.; Parot, Y.; Pérez, R.; Pinet, P.; Poitrasson, F.; Quertier, B.; Sallé, B.; Sotin, C.; Sautter, V.; Séran, H.; Simmonds, J. J.; Sirven, J. B.; Stiglich, R.; Striebig, N.; Thocaven, J. J.; Toplis, M. J.; Vaniman, D. *Space Sci. Rev.* **2012**, *1–72*.
- (68) Wiens, R. C.; Maurice, S.; Clegg, S. M.; Sharma, S. K.; Misra, A. K.; Bender, S.; Newell, R.; Dallmann, N.; Lanza, N.; Forni, O.; Lasue, J.; Rull, F. *43rd Lunar Planet. Sci. Conf. (2012)* **2012**, 1699.
- (69) Strazzulla, G.; Baratta, G. A.; Palumbo, M. E. *Spectrochim. Acta, Part A* **2001**, *57* (4), 825–842.